The 11th Canadian Conference on Earthquake Engineering
Canadian Association for Earthquake Engineering

A STUDY ON THE ROTATIONAL BEHAVIOUR OF BONDED AND UNBONDED FIBER REINFORCED ELASTOMERIC ISOLATORS

Yasser Al-Anany
Ph.D. Candidate, McMaster University, Canada
alananym@mcmaster.ca

Michael J. Tait
Associate Professor, JNE Consulting Chair in Design, Construction, and Management in Infrastructure Renewal
McMaster University, Canada
taitm@mcmaster.ca

ABSTRACT: Fiber reinforced elastomeric isolators (FREI) use fabric instead of steel as the reinforcement material. Fiber reinforced elastomeric isolators can be classified as either bonded or unbonded. Bonded FREI (B-FREI) have thick steel end plates that are fastened to the superstructure and the foundation. Unbonded FREI (U-FREI) are constructed without thick steel end plates and are placed, unfastened, between the superstructure and the foundation. A number of studies have focused on the response of FREI base isolated buildings under seismic excitation. However, the performance of FREI when installed in other types of structures, such as bridges, has not been investigated to the same extent. When employed for the seismic isolation of a bridge, the rotational behaviour of the isolator must also be considered. A comparative study on the response of B-FREI and U-FREI subjected to rotational deformations is presented. The response of B-FREI and U-FREI are obtained through 2D FE analysis. All the investigated isolators have the same width and height, but different shape factor values. Results from FE analysis are examined to assess the influence of shape factor on the rotational behaviour of B-FREI and U-FREI.

1. Introduction

Seismic isolators are considered a critical element, as they are the only link between bridge superstructure (girders) and substructure (piers/abutments) and, as such, must be able to accommodate the vertical, lateral, and rotational deformations that are expected to occur during the lifetime of the bridge (Lee, 1994). Seismic isolators must possess sufficient vertical stiffness in order to adequately resist and transmit gravity loads from superstructure to substructure. In addition, they must be able to accommodate movement induced in the girders due to temperature, shrinkage, creep, traffic, wind and seismic forces, while possessing sufficient flexibility in the lateral direction. Finally, they must be capable of accommodating rotations induced by both dead and live loads (OPSS 1202, 2008 and 1203, 2008).

Over the past 70 years the demand on bridge bearings has increased due to rapid developments in bridge design, such as the introduction of frames with much larger spans and innovative forms (i.e. curved and skewed) (Caltrans, 1994). Elastomeric bearings and high load multi-rotational bearings (pot, spherical, and disk) are the most common types of bearings used in bridge applications (Ramberger, 2002). The selection of the bearings type depends on several factors such as loads, geometry, maintenance, available clearance, deflection, displacement, rotation, availability, policy, designer preference, and cost (Caltrans, 1994 and OPSS 922, 2009).

Typically, elastomeric bearings/isolators are reinforced with steel plates/shims, which result in a high vertical stiffness by limiting the bulging in elastomer layers. This type of isolator is called a Steel Reinforced Elastomeric Isolator (SREI). When fiber material is used as the reinforcement, instead of steel,

the isolators are denoted as Fiber Reinforced Elastomeric Isolators (FREI). Bonded FREI (B-FREI) are connected to the superstructure and the foundation through top and bottom thick end plates, while unbonded FREI (U-FREI) are simply placed between the superstructure and its foundation without rigid end plates.

Relative to U-FREI, SREI are heavy due to the rigid steel end plates and steel reinforcement shims, which result in isolators weighing up to one ton or more (Kelly and Konstantinidis, 2007). Replacing the steel reinforcement with lighter fiber material and removing the rigid end plates can result in a significant reduction in weight. The fiber reinforcement and elastomer can be effectively bonded together using cold-vulcanization without the need of a specialized mold. Furthermore, the manufacturing cost has the potential to be significantly reduced as individual isolators can be cut from large sheets using a standard band saw. FREI possess unique advantages over SREI, including ease of installation, negligible flexural rigidity, superior damping properties, high seismic isolation efficiency and lower stresses in the elastomer and fiber (Toopchi-Nezhad et al., 2008 (a & b)).

A number of numerical studies using finite element (FE) analysis have been carried out in order to investigate the response of B-FREI and U-FREI under vertical and lateral loads/deformations. Mordini and Strauss (2008) performed a FE study on FREI to investigate the effects of various parameters, including boundary conditions, on the response behaviour. Toopchi-Nezhad et al. (2012) studied the influence of the shape factor, which represents the ratio of loaded area to free bulging area, on the lateral response of U-FREI. Osgooei et al. (2014) conducted a three-dimensional FE analysis study on the vertical response characteristics of circular FREI. However, to date the response of FREI under rotational loads/deformations has not received the same level of attention. That is because most of the research work completed has focused on the isolation of structures, which do not induce rotational deformations. The objective of this study is to gain insight into the behaviour of FREI when both vertical and rotational loads/deformations are applied in combination. The findings presented here are part of a larger research program investigating the viability of FREI for bridges, which according to CAN/CSA-S6 Canadian Highway Bridge Design Code (CHBDC) (CSA 2006) and the American Association of State Highway and Transportation Officials (AASHTO) LRFD Bridge Design Specifications, (AASHTO 2012) must transmit loads while facilitating translation and/or rotation.

2. Finite Element Analysis

In this study, FE analysis has been employed to study infinitely long strip FREI under rotational deformation. The primary goal of the FE analysis is to investigate the rotational behaviour of FREI with bonded (B-FREI) and unbonded (U-FREI) boundary conditions in order to evaluate the performance of isolators with different shape factors subjected to different angles of rotation and assess the resulting stress and strain state. A two-dimensional FE analysis, under the plane strain assumption, was completed using the commercially available general-purpose finite element program MSC Marc (MSC Software, 2013). A schematic of a representative isolator, indicating the overall dimensions, is shown in Fig. 1.

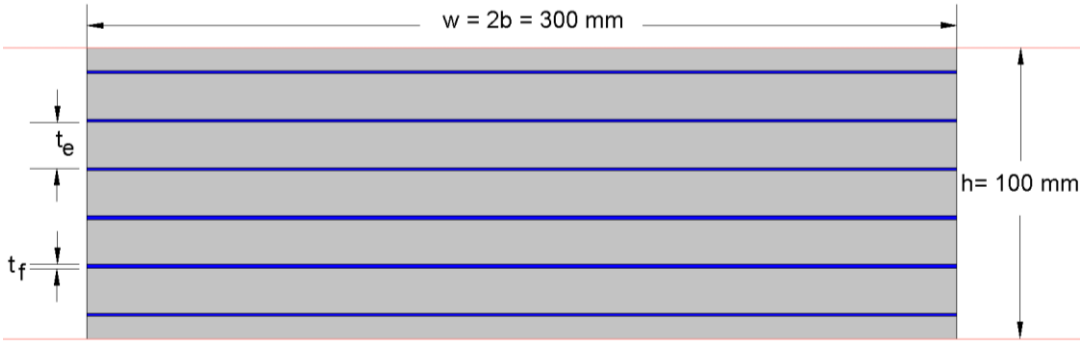

Fig. 1: Schematic of Isolator

Two rigid wires were defined at the top and bottom of the isolators to represent the contact supports. The upper rigid wire had a control node with one degree of freedom in the vertical direction. Rotations were

imposed through the upper rigid wire using an auxiliary node that had a single rotational degree of freedom. The “Glue” and “Touching” contact models were selected to simulate the contact conditions between the contact supports for the B-FREI and U-FREI, respectively. For the U-FREI, the shear force between the contact supports and the isolator was transferred through Coulomb friction using an assumed friction coefficient of 1.0. All isolators were first vertically loaded through the upper rigid wire until the target mean vertical pressure was achieved. Rotations were subsequently applied through the upper rigid wire.

Table 1 shows the geometric properties of the modelled isolators. The parameter varied in this study was the shape factor (S). For a strip isolator the shape factor is given by

$$S = \frac{w}{2t_e} = \frac{b}{t_e} \tag{1}$$

Isolators with three different shape factor values, as shown in Table 1, were considered in this study. The selected values for (S) were 9.6, 20.5, and 32.9. These values cover the range of shape factor values for elastomeric isolators that are typically employed for the seismic isolation of bridges (Konstantinidis et al., 2008). All isolators had the same aspect ratio of 3.0, which is defined as the ratio between the isolator width (w) and height (h) (see Fig. 1). The mean vertical pressure (P) value used in this study was 7 MPa, which represents the intermediate limit between the serviceability limit state (SLS) and ultimate limit state (ULS) in the CHBDC (CSA 2006) and the intermediate limit between Methods A & B for the design of bridges according to LRFD Bridge Design Specifications (AASHTO 2012). The maximum imposed angle of rotation was 0.05 radians, which is the expected maximum value for steel girder bridges.

Table 1 – Isolator Geometric Properties

	Isolator 1	**Isolator 2**	**Isolator 3**
Fiber Layer Thickness, t_f (mm)	1	1	1
Total Fiber Layers	6	12	18
Total Fiber Thickness (mm)	6	12	18
Total Elastomer Thickness, t_r (mm)	94	88	82
Number of Elastomer layers including cover	7	13	19
Intermediate Elastomer Layer Thickness, t_e (mm)	15.66	7.33	4.55
Cover Elastomer Layer Thickness (mm)	7.83	3.66	2.27
Shape Factor, S	9.6	20.5	32.9
Half Isolator Width, b (mm)	150		
Total Isolator Height, h (mm)	100		
Aspect Ratio	3		
Out of Plane Thickness (mm)	1		

The elastomeric and fiber layers were modelled using 4-node quadrilateral elements developed for plane strain analysis. A hyperelastic Neo-Hookean material model was used to represent the elastomer material as shown in Table 2. This model is defined by two parameters: the shear modulus, G_e, and bulk modulus, K_e. A linear elastic isotropic material, defined by two constants: the elastic modulus, E_f, and Poisson’s ratio, v_f, were used to model the reinforcement.

Table 2 – Material Properties

Elastomer	**Fiber**
Shear Modulus, G_e = 0.80 MPa	Elastic Modulus, E_f = 30 GPa
Bulk Modulus, K_e = 2000 MPa	Poisson’s ratio, v_f= 0.20

3. Analysis of Results and Discussions

3.1. Moment-Rotation Response

Fig. 2 compares the moment-rotation response curves, obtained from FE analysis, for both the B-FREI and U-FREI. As shown, the B-FREI maintains a linear moment-rotational relationship until excessive deformation in the reinforcement, located in the portion of the bonded isolator that experiences tensile stresses in the elastomer, occurs. This results in a significant reduction in the rotational capacity of the isolator. By examining Fig. 2 it can be observed that the behaviour of U-FREI under rotational deformation can be divided into two phases. In the first phase, under small angles of rotation, the moment-rotation behaviour is linear. The rotational response of U-FREI in this phase is consistent with that of B-FREI as the top and bottom contact surfaces maintain full contact. Conversely, in the second phase, which occurs at higher angles of rotation, the isolator response is nonlinear. The significant reduction in the rotational stiffness is due to the loss of contact area between the isolator and the supports as a result of the unbonded boundary conditions between the isolator and the top and bottom support surfaces (i.e. geometric nonlinearity). This loss of contact is referred to as lift-off (Mori et al., 1999).

The rotational stiffness of an isolator must be evaluated to ensure that it can accommodate the expected load-induced rotations and that it satisfies stability requirements (Stanton, 2008). In addition, the rotational stiffness influences the critical buckling load of an isolator (Kelly and Konstantinidis, 2011). According to Tsai and Kelly (2001), the rotational stiffness, K_θ, of an isolator subjected to a an angle of rotation, θ, due to a bending moment, M, can be expressed as

$$K_\theta = \frac{M}{\theta} = \frac{(EI)_{eff}}{t_r} \tag{2}$$

where, the effective bending stiffness, $(EI)_{eff}$, for strip isolators is defined as

$$(EI)_{eff} = \frac{24 G_e S^2}{\alpha^4 b}\left(1 + \frac{1}{3}(\alpha b)^2 - \frac{\alpha b}{\tanh(\alpha b)}\right) \tag{3}$$

The parameter α in Eq. (3) is a function of the reinforcement flexibility

$$\alpha = \sqrt{\frac{12 G_e (1 - \nu_f{}^2)}{E_f t_f t_e}} \tag{4}$$

As shown in Fig. 2, good agreement is found between the rotational response of B-FREI and U-FREI obtained from FE analysis and the analytical solution given by Eq. (2) for small rotations. For U-FREI, agreement with Eq (2) is expect only for small rotations (prior to the initiation of lift-off) when full contact is maintained between the isolator and the upper and lower supports. From Eq (3), it can be observed that the rotational stiffness of an isolator increases quadratically with the shape factor. As a result, the initiation of lift-off is expected to occur under lower rotational values as the effective bending stiffness increases due to an increase in the shape factor. The results presented in Fig. 2 confirm this expected behaviour.

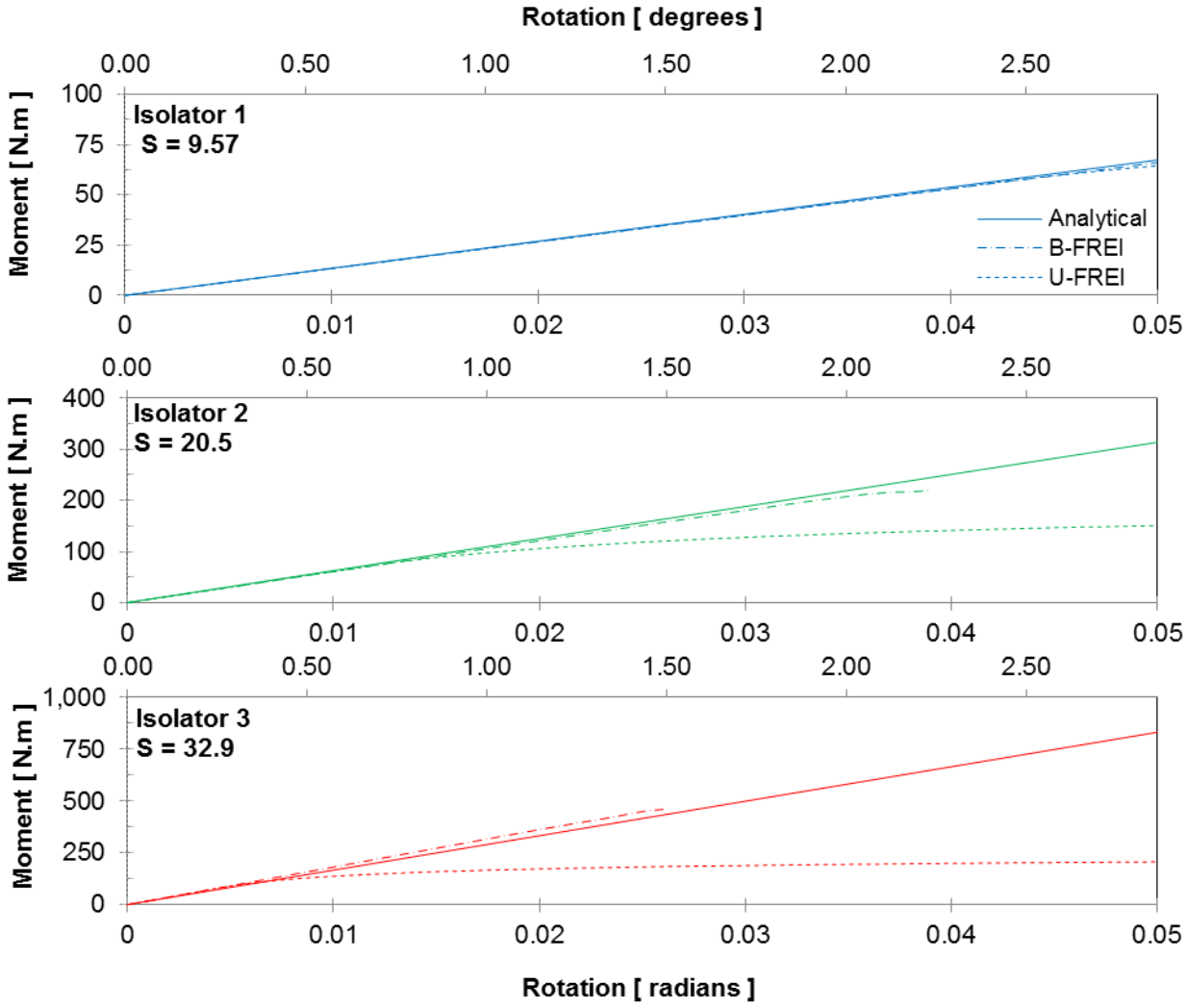

Fig. 2 – Moment-Rotation Response

This section presents the vertical (σ_{22}) and lateral (σ_{11}) stresses that develop in the elastomer layers. Fig. 3 presents the evolution of normalized stress distribution (σ/P) along the length of the intermediate elastomer layer. Stresses are shown for an applied mean vertical pressure of 7 MPa, and at angles of rotation: $\theta = 0$ (i.e. pure compressive stress of 7 MPa), 0.01 and 0.025 rad. As shown in Fig. 3, the magnitude of compressive stresses increases, in both the B-FREI and U-FREI, with increased rotation because of the additional compressive stress induced as a result of the applied rotation. Furthermore, for the U-FREI, the loaded area decreases (as a result of lift-off) as the applied angle of rotation is increased.

It can be observed that as the applied angle of rotation is increased, the deviation in the peak compressive stress value for the B-FREI and U-FREI increases, with lower peak stress values occurring in the U-FREI. Moreover, at higher angles of rotation, significant tensile stresses develop on one side of the B-FREI compared to the development of negligible tensile stresses in the U-FREI. This is because no loss of contact (lift-off) is permitted for the B-FREI, while for the U-FREI lift-off is allowed. Additionally, for both the B-FREI and U-FREI studied, negligible difference can be observed between the distribution and peak values of stresses σ_{11} and σ_{22}, even at higher angles of rotation. This confirms that the pressure solution assumption that the elastomer is in a hydrostatic state of stress (i.e. $\sigma_{11} = \sigma_{22} = P_{hydrosatic}$) is valid.

Results presented in Fig. 3 show that biaxial compression is developed in the compressed side of the isolator, while the uncompressed side is subjected to biaxial tension. According to Fig. 3, the biaxial tension is significant for B-FREI and is negligible for U-FREI.

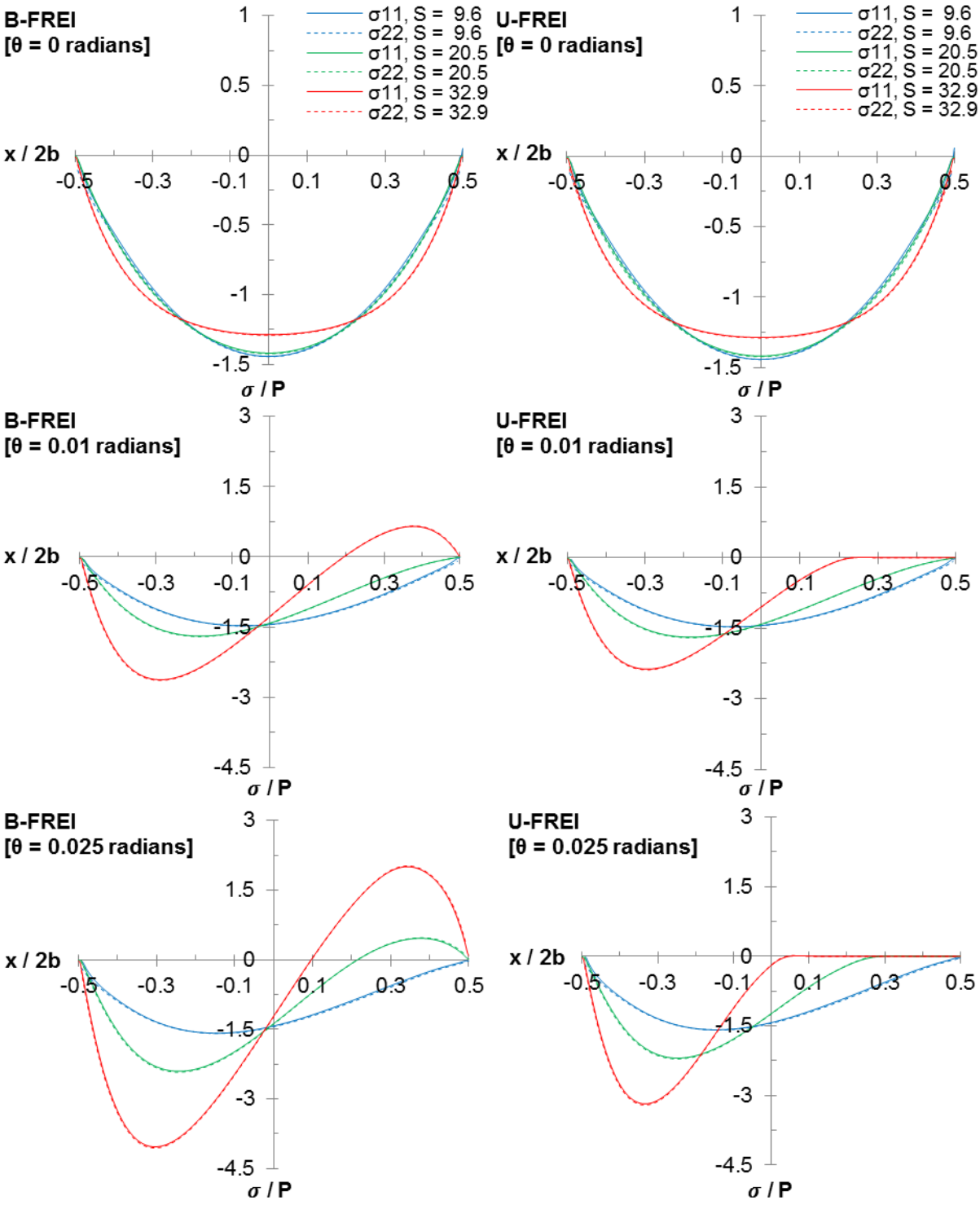

Fig. 3 – Profile of Normalized Stress Distribution Along the Top Surface of the B-FREI and U-FREI

The variation of peak stresses (σ_{max}) developed in the elastomer layer for all six isolators considered in this study when subjected to rotations up to 0.05 radians are shown in Fig. 4. The stresses are normalized with respect to the applied mean vertical pressure of 7 MPa. It can be observed from Fig. 4 that the maximum stress, σ_{max}, which develops due to rotation, is always lower in the U-FREI compared to the corresponding B-FREI. Additionally, the increase in σ_{max}, as a result of applied rotation, is significantly less for isolators with low shape factors. This is due to the increased vertical and rotational

flexibility characteristics resulting from the bulging in the load free surfaces because of the reduced confinement. Conversely, isolators with higher shape factor values possess higher vertical and rotational stiffness values. As a result, the loss of compressive contact area occurs at much lower applied rotational values. According to Fig. 4, at θ = 0.025 radians, the peak normalized compressive stresses ($\sigma_{22,max}$/P) for the B-FREI are approximately 0.01%, 9%, and 45% higher than for the corresponding U-FREI with shape factors of 9.6, 20.5 and 32.9, respectively.

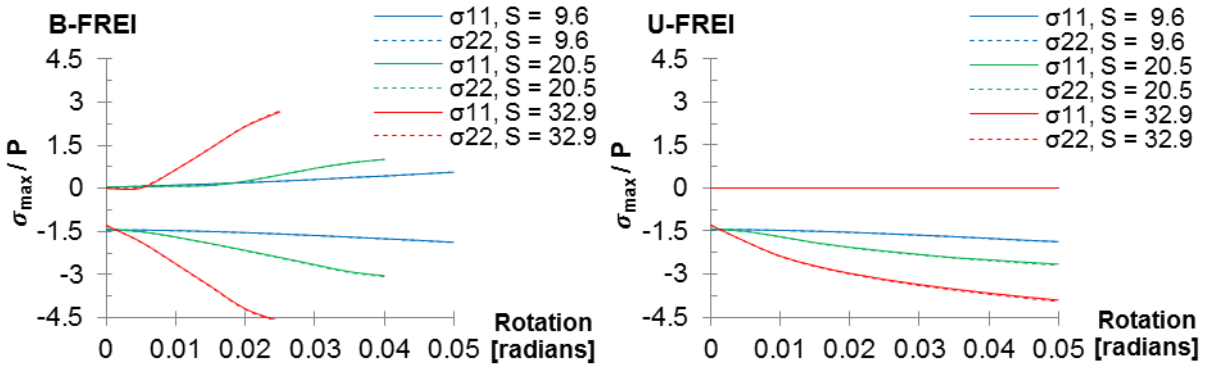

Fig. 4 – Variation of Peak Stresses (σ_{11} & σ_{22})

3.2. Shear Strain in the Elastomer

Delamination of the elastomer from the reinforcement is considered one of the most critical modes of failure (Stanton, 2008). The variation of peak shear strain values developed in all isolators under different angles of rotation is plotted in Fig. 5. It can be observed that under pure compression, even though the value of shear strain is not affected by the end boundary conditions, it is highly dependent on the shape factor. For example, the maximum shear strain value decreases by a factor of 3.6 when the shape factor is increased from 9.6 to 32.9. Moreover, the shear strain between the elastomer layers and reinforcement increases as the angle of rotational is increased. This increase in shear strain is more pronounced in isolators with a lower shape factor. For instance, under pure compression the peak value of shear strain in the isolators with S = 20.5 is approximately equal to 0.28. However, when an angle of rotation of 0.04 radians is applied, it experiences an increase of approximately 518% for the B-FREI. For U-FREI, under the same rotation of 0.04 radians, the peak shear strain value increases by 285%.

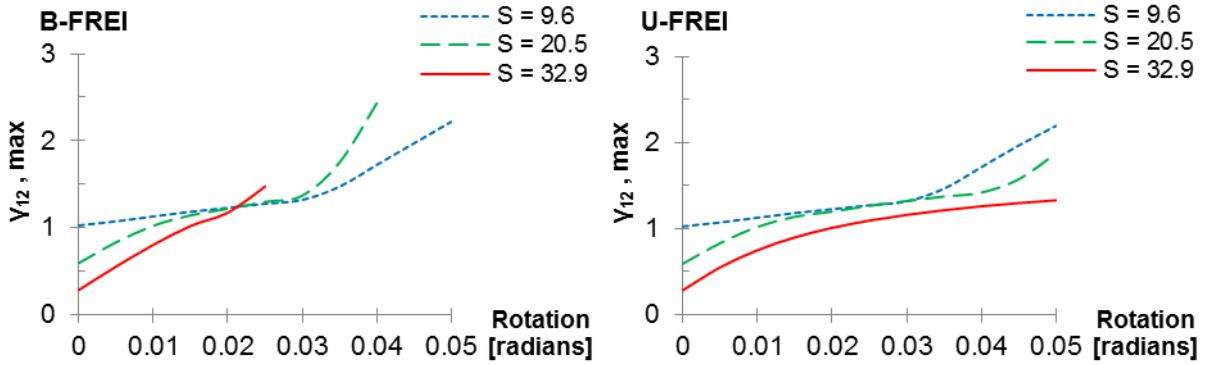

Fig. 5 – Variation of Peak Shear Strain (γ_{12})

3.3. Tensile Strain in the Reinforcement

Introducing reinforcement layers to confine the elastomer layers allows a relatively high compressive stiffness to be achieved, which mitigates the excitation of rocking modes. As shown in Fig. 6, tensile or compressive strains can occur in the fiber reinforcement depending on the stresses that develop in the confined elastomer layer. From Fig. 6(a) it can be observed that when the isolator is under compression

loading tensile strains are introduced in the fiber reinforcement, which limits bulging in the elastomer layers. Conversely, when the elastomer is under tension loading (Fig. 6(b)), compressive strains develop in the fiber reinforcement.

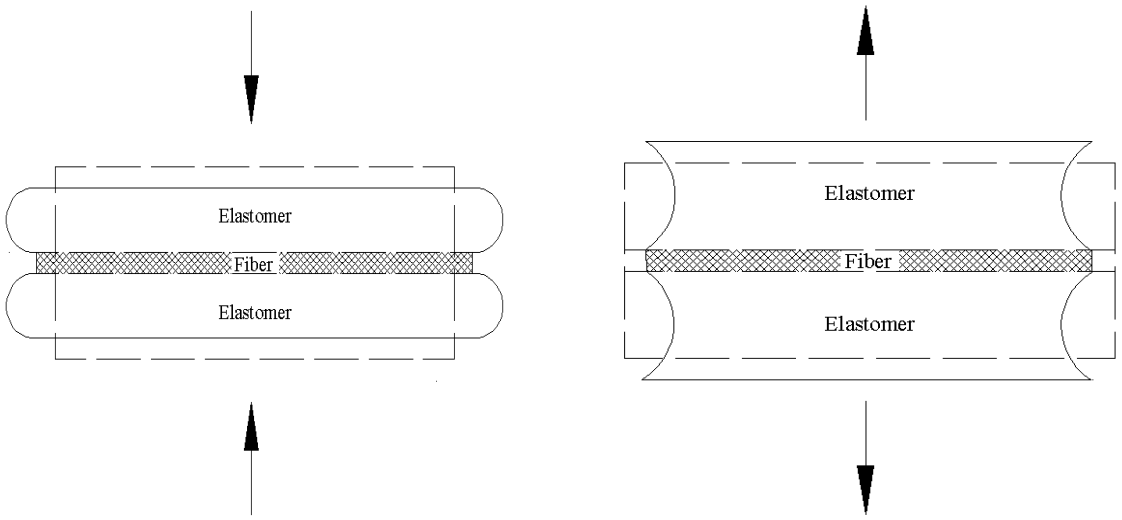

(a) Tensile strain in fiber **(b) Compressive strain in fiber**

Fig. 6 – Deformation of Elastomer and Fiber Reinforcement Under Vertical Load

Fig. 7 presents the peak strains that develop in the fiber reinforcement for different levels of applied rotation. It is observed that the peak magnitudes of fiber strain are the same for the B-FREI and U-FREI when subjected to a pure compressive load. The peak fiber strain in the B-FREI, with higher shape factors (20.5 and 32.9), increases more rapidly compared to the U-FREI as the applied rotation is increased. The larger increase in the compressive fiber strain for the B-FREI occurs because portions of the elastomer layers in the uncompressed side of the isolator are subjected to high tensile stresses. This high compressive strain in the fiber reinforcement results in excessive distortion (buckling) of the fiber reinforcement. It is important to note that the fiber will not yield when it buckles and, as such, it is expected to return its original shape upon unloading with no permanent damage to the fiber. On the other hand, for U-FREI, the fiber deforms as a result of the deformation induced by the applied rotation, leading to the development of compressive strains in fiber, which are much smaller than the compressive strains in the B-FREI.

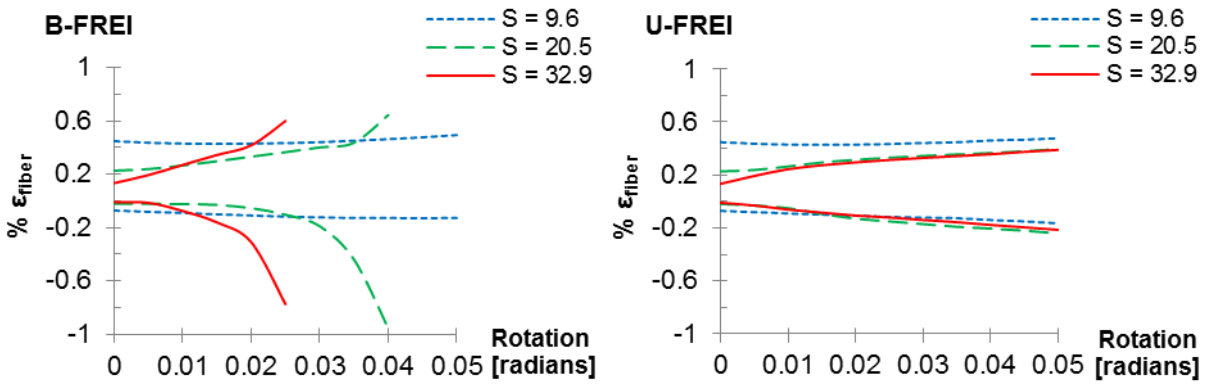

Fig. 7 – Variation of Peak Strain in Fiber Reinforcement (%ε_{fiber})

Under pure compression, the peak fiber strain is identical in isolators with the same shape factor, regardless of the end boundary condition. The shape factor affects the values of stress that develop in each elastomer layer and the corresponding tensile strain in the fiber reinforcement for a given applied

vertical load. Therefore, isolators with higher shape factor values are expected to experience lower tensile strains in the fiber reinforcement relative to isolators with lower shape factor values. Additionally, the rate of increase in peak fiber strain due to rotation is strongly affected by the shape factor and the end boundary conditions. For example, the peak compressive strain value for the isolators having S = 20.5 is approximately -0.02% under pure compression, however, when an angle of rotation of 0.04 radians is applied the peak compressive strain increases to -0.95% for B-FREI and -0.24%, for U-FREI.

4. Summary and Conclusions

The main objective of this study was to gain a better understand the behaviour FREI when vertical and rotational loads/deformations are applied in combination. To achieve this objective, finite element (FE) analysis was carried out on FREI under vertical and rotational loading. The FREI were modelled to simulate both bonded and unbonded boundary conditions between the isolator and the top and bottom supports. The primary goal of the FE analysis was to investigate the vertical and rotational behaviour of FREI in order to evaluate the performance of isolators with different shape factors subjected to different angles of rotation, and assess the resulting stress and strain states. The isolators investigated had shape factor values of 9.6, 20.5 and 32.9, respectively, while the aspect ratio for all isolators was held constant. All isolators were vertically loaded up to a mean compressive pressure of 7 MPa, and rotationally deformed up to a maximum value of 0.05 radians. Excellent agreement was found between the results of the conducted FE analysis with the analytical solution “pressure solution” approach.

Based on the FE results, the following advantages are drawn for the rotational response of the modelled U-FREI compared to that of the B-FREI:

- the ability to accommodate higher angles of rotation.
- the compressive stress that develops in elastomer is lower, and the tensile stress is negligible.
- the tensile and compressive strain that develops in the fiber reinforcement is significantly lower.

Moreover, it was noted that the shape factor has a significant effect on the:

- normal stresses in the elastomer.
- strains in the reinforcement.

Finally, it is important to note that the shape factor and the end boundary conditions affect the rate of increase in the magnitude of stress and strain in the isolator.

Ongoing research is being carried out to experimentally investigate the rotational behaviour of U-FREI. It would also be valuable to study the behaviour of isolators when lateral deformation is applied, in addition to vertical and rotational deformations, in order to evaluate the viability of FREI in bridges.

5. Acknowledgements

This research was carried out as part of the mandate of the McMaster University Centre for Effective Design of Structures funded through Ontario Research and Development Challenge Fund. The authors also would like to gratefully acknowledge the Natural Sciences and Engineering Research Council of Canada (NSERC).

6. References

AASHTO. American Association of State Highway and Transportation Officials. LRFD Bridge Design Specifications, Washington, D.C, 2012.

CAN/CSA-S6-06. Canadian Highway Bridge Design Code. Canadian Standards Association. Mississauga, Ontario, 2006.

Caltrans. Bridge Memo to Designers. Section 7: Bridge Isolators. California Department of Transportation, Sacramento, California, 1994.

Kelly JM, Konstantinidis D, “Low-Cost Seismic Isolators for Housing in Highly Seismic Developing Countries”, *ASSISi 10th World conference on seismic isolation, energy dissipation and active vibrations control of structures*, Istanbul, May 2007, pp. 28–31

Kelly JM, Konstantinidis D, *Mechanics of rubber isolators for seismic and vibration isolation*. Chichester, UK: Wiley, 2011.

Konstantinidis D, Kelly JM, Makris N, *Experimental Investigations on the Seismic Response Of Bridge Bearings.* Report No. EERC-2008/02, Earthquake Engineering Research Center, University of California, Berkeley; 2008.

Lee, David J, *Bridge Isolators and Expansion Joints*. E & FN Spon, London, UK, 1994.

Mordini A, Strauss A, “An Innovative Earthquake Isolation System Using Fibre Reinforced Rubber Bearings”, *Engineering Structures*, 2008, Vol. 30, pp. 2739-51.

Mori A, Moss P, Cooke N, and Carr A, “The Behavior of Isolators Used for Seismic Isolation Under Rotation and Axial Load”. *Earthquake Spectra*, 1999, Vol.15, No. 2, pp. 225–44.

MSC Software (2013). MSC Marc 2013, Santa Ana, CA.

OPSS 922, MTO, Construction Specification For Installation Of Isolators. Ontario Ministry of Transportation, Toronto, Ontario, 2009.

OPSS 1202, MTO, Material Specification for Isolators – Elastomeric Plain and Steel Laminated. Ontario Ministry of Transportation, Toronto, Ontario, 2008.

OPSS 1203, MTO, Material Specification for Isolators – Rotational and Sliding Surface. Ontario Ministry of Transportation, Toronto, Ontario, 2008.

Osgooei PM, Tait MJ, Konstantinidis D, “Three-Dimensional Finite Element Analysis of Circular Fiber-Reinforced Elastomeric Bearings Under Compression”, *Composite Structures*, 2014, Vol. 108, pp. 191–204.

Ramberger G, *Structural Isolators and Expansion Joints for Bridges, International Association for Bridges and Structural Engineering*. IABSE, Zurich, Switzerland, 2002.

Stanton J, Roeder C, Mackenzie-Helnwein P, White C, Kuester C, Craig B, *Rotation Limits for Elastomeric Isolators.* Report No. NCHRP 596, Transportation Research Board, National Cooperative Highway Research Program, Washington, D.C., 2008

Toopchi-Nezhad H, Tait MJ, Drysdale RG, “Testing And Modeling of Square Carbon Fiber-Reinforced Elastomeric Seismic Isolators”, *Structural Control Health Monitoring*, 2008, Vol. 15, No. 6, pp. 876–900.

Toopchi-Nezhad H, Tait MJ, Drysdale RG, “Lateral Response Evaluation of Fiber-Reinforced Neoprene Seismic Isolators Utilized in an Unbonded Application”, *Journal of Structural Engineering*, 2008, Vol. 134, No. 10, pp.1627–37.

Toopchi-Nezhad H, Drysdale RG, Tait MJ, “Influence of Thickness of Individual Elastomer Layers (First Shape Factor) on the Response of Unbounded Fiber-Reinforced Elastomeric Bearings*”, Journal of Composite Material*, 2012, Vol. 47, No. 27, pp. 3433-50.

Tsai HC, Kelly JM, *Stiffness Analysis of Fiber-Reinforced Elastomeric Isolators*. Pacific Earthquake Engineering Research Center, PEER, Berkeley, California, 2001.